Eur. Phys. J. B (2016) 89: 90
DOI: 10.1140/epjb/e2016-60585-9

THE EUROPEAN PHYSICAL JOURNAL B

Regular Article

Structural stability and electronic properties of $AgInS_2$ under pressure

G.M. Dongho Nguimdo[1,a], George S. Manyali[1,2], Mahmud Abdusalam[1], and Daniel P. Joubert[1]

[1] National Institute for Theoretical Physics, Mandelstam Institute for Theoretical Physics, School of Physics, University of the Witwatersrand, Private Bag 3, 2050 Johannesburg, South Africa
[2] Computational and Theoretical Physics Group, Physics Department, Masinde Muliro University of Science and Technology, P.O Box 190-50100, Kakamega, Kenya

Received 20 July 2015 / Received in final form 14 November 2015
Published online 6 April 2016 –

Abstract. We employ state-of-the-art ab initio density functional theory techniques to investigate the structural, dynamical, mechanical stability and electronic properties of the ternary $AgInS_2$ compounds under pressure. Using cohesive energy and enthalpy, we found that from the six potential phases explored, the chalcopyrite and the orthorhombic structures were very competitive as zero pressure phases. A pressure-induced phase transition occurs around 1.78 GPa from the low pressure chalcopyrite phase to a rhombohedral RH-$AgInS_2$ phase. The pressure phase transition around 1.78 GPa is accompanied by notable changes in the volume and bulk modulus. The calculations of the phonon dispersions and elastic constants at different pressures showed that the chalcopyrite and the orthorhombic structures remained stable at all the selected pressure (0, 1.78 and 2.5 GPa), where detailed calculations were performed, while the rhombohedral structure is only stable from the transition pressure 1.78 GPa. Pressure effect on the bandgap is minimal due to the small range of pressure considered in this study. The meta-GGA MBJ functional predicts bandgaps which are in good agreement with available experimental values.

1 Introduction

Ternary chalcogenide materials are among the semiconductor materials which have recently received attention from the scientific community [1–9] due to their potential technological applications. As other chalcopyrite materials, the tetragonal (chalcopyrite) phase of $AgInS_2$ compound is very attractive in the electronic and optoelectronic industries [10,11]. Both the orthorhombic and the chalcopyrite structures of $AgInS_2$ are ideal photocatalyst materials for water splitting [12–17]. With their bandgap (1.86–1.98 eV) and absorption coefficients, they are also suitable materials to be used as visible light absorber layers and outer shell sensitizers of multi junction solar cells [10,18]. Moreover, they are direct bandgap semiconductors and their electronic and optical properties can easily be tuned by doping or by stress [14–17,19,20]. Contrary to the chalcopyrite $AgInS_2$, a limited number of experimental and theoretical studies have been performed on the orthorhombic $AgInS_2$.

In the early seventies, Range et al. [20] investigated high pressure transformations of ternary chalcogenides and observed a high pressure rhombohedral phase of $AgInS_2$, but their study was limited to structural properties. To the best of our knowledge further studies on this phase have not been performed so far neither theoretically nor experimentally. Using an energy dispersion technique, Werner et al. [21] found that the chalcopyrites $CuGaS_2$ and $AgGaS_2$ undergo pressure-induced phase changes from chalcopyrite to a NaCl type structure at pressures near 15 GPa. DFT calculations by Addellaoui et al. [22] predicted a structural phase transition of $CuAlX_2$ (X = S, Se, Te) materials from the chalcopyrite phase to the rocksalt phase at pressures below 14 GPa. Because of the potential applications of chalcopyrite $AgInS_2$ and the aforementioned reasons, a more complete study of this family of compounds need to be done. Here we perform a detailed study of observed and hypothetical structural phases of $AgInS_2$ including chalcopyrite, tetragonal, orthorhombic, hexagonal, rocksalt (NaCl) and monoclinic configurations.

2 Methodology

All our calculations are carried out within the framework of Density Functional Theory (DFT) using the VASP code [23]. The electron-ion interaction is described by the projecter augmented wave (PAW) formalism [24]. For the exchange-correlation interaction, we used the GGA-PBEsol [25] generalised gradient approximation (GGA) and the modified Becke-Johnson potential (MBJ) [26]. Since the MBJ potential is not a functional derivative of

[a] e-mail: donghomoise@gmail.com

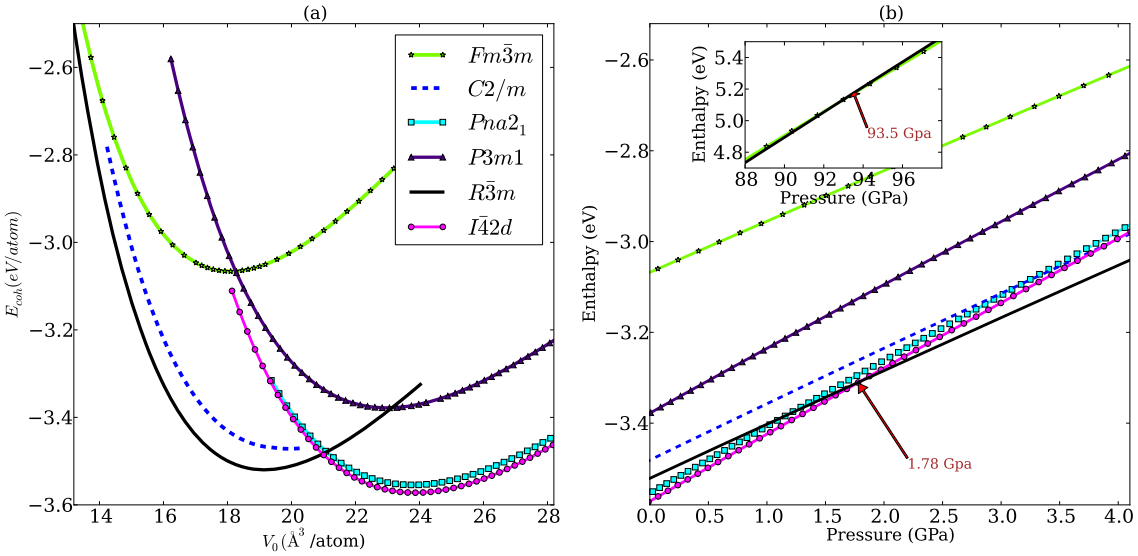

Fig. 1. Cohesive energy versus volume (a) and enthalpy versus pressure (b) for the chalcopyrite ($I\bar{4}2d$), the monoclinic $C2/m$, the orthorhombic $Pna2_1$, the trigonal $P3m1$, the trigonal $R\bar{3}m$ and the rocksalt $Fm\bar{3}m$ structures.

an energy functional [27], all the structural optimizations were performed with the GGA-PBEsol functional only. The advantage of the meta-GGA MBJ is that it usually overcomes the failure of GGA functionals in predicting the bandgap at a reasonable computational cost when compared to hybrid functional [28] and GW [29] methods.

For predicting a potential high pressure stable structural phase, we consider a rocksalt (NaCl) structure with space group $Fm\bar{3}m$ (No. 225), an orthorhombic structure with space group $Pna2_1$ (No. 33), a rhombohedral structure with space group $R\bar{3}m$ (No. 166), a hexagonal structure with space group $P3m1$ (No. 156) and a monoclinic phase with space group $C2/m$ (No. 12) in addition to the well known and well studied chalcopyrite $AgInS_2$ phase with the space group $I\bar{4}2d$ (No 122). Details on the structures can be obtained using the identification numbers (IDs) from the materials project (MP) [30] or the inorganic crystal structure database (ICSD) [31] as listed in Table 1. The selection of these structures was based on previous experimental and theoretical studies on similar families of materials including the $CuAlX_2$, the $AgAlX_2$ and the $ZnSiP_2$ compounds and $AgInX_2$ itself [8,9,20,22,30,32].

Plane waves with kinetic energy up to 550 eV were considered in the calculations. For the sampling of the Brillouin Zone (BZ), Monkhorst-Pack [33] **k**-points meshes with grids of $7 \times 7 \times 7$ were used for the tetragonal, the rhombohedral and the rocksalt phase while $6 \times 6 \times 6$, $8 \times 8 \times 6$ and $4 \times 9 \times 8$ were used for the orthorhombic, the hexagonal and the monoclinic phases. These parameters were found to be sufficient for energy convergence to within 0.1 meV per atom. Full ionic relaxation of all the structures were performed until the total energy was converged to within 0.1 meV. To remain in the harmonic approximation, small distortions of ± 0.01 Å were allowed for the elastic constant calculations. Force constants were calculated using density functional perturbation theory (DFPT) [34] as implemented in the VASP code. Phonon dispersion relations were obtained from the force constants by means of the PHONOPY code [35,36]. The coordinates of the high symmetry **k**-points in the Brillouin zones for bandstructure and phonon dispersion curves calculations were automatically generated from AFLOW software [37].

3 Results and discussions

3.1 Structural and energetic properties

We started by performing full relaxation calculations of volume, shape and atomic positions for all the structures while keeping the lattice type constant. Then a set of self-consistent calculations at different volumes spanning each predicted equilibrium volume V_0 were carried out and a third order Birch-Murnaghan [38] equation of state (EOS) was fitted to the obtained energies as depicted in Figure 1. Information extracted from the (EOS) fits are summarized in Table 1. Comparison to other calculated and experimental results shows that the lattice parameters and equilibrium volume are in general agreement with our results. Being ternary analogues of the binary zincblende structures, chalcopyrite structures are defined by two extra parameters in addition to the lattice parameters, known as tetragonal distortion $\eta = c/2a$ and anion displacement u [39]. We obtained $\eta = 0.970$ and $u = 0.250$ which are in agreement with experimental data ($\eta = 0.960$ and $u = 0.250$) [39]. The equilibrium volume V_0 of the orthorhombic (OR-$AgInS_2$) structure is slightly larger than that of the tetragonal chalcopyrite phase (CH-$AgInS_2$). This trend is confirmed by the experimental results. From Table 1 it can also be seen that the bulk modulus for the OR-$AgInS_2$ structure is the smallest while the rocksalt structure has the largest bulk modulus of the calculated values. The bulk modulus B_0 of CH-$AgInS_2$ (62 GPa) is in the range of the previously

Table 1. Crystallographic description and zero pressure and temperature structural parameters of the six structural phases of $AgInS_2$ studied using the GGA-PBEsol functional. The space group, the space group number (in square brackets) and the prototype structures are given as indication for the structures under investigation. Details about the structures can be found using the identification numbers (IDs) from the Materials Project (MP) [30] or the Inorganic Crystal Structure Database (ICSD) [31] where available. For the rocksalt-type structure, there are 1 Copper atom, 1 Aluminium and 2 Sulfur atoms respectively at 4a, 4b and 8c Wyckoff positions, i.e. Cu(0.0,0.0,0.0), Al(0.5,0.5,0.5) and X(0.25,0.25,0.25) gotten from reference [22]. Lattice parameters a, b, c are given in Å, the volume per atom V_0 in $Å^3$, the bulk modulus B_0 in GPa, the gravimetric density ρ in $g.cm^{-3}$ and the cohesive energy per atom E_{coh} and the formation energy per atom E_{for} in eV. The present calculations are compared to previous calculated (Calc.) and experimental data (Exp.) where available.

Phase	Space Group	MP or ICDS IDs	Prototype	a	b	c	V_0	ρ	B_0	E_{coh}	E_{for}
Tetragonal (CH)	$I\bar{4}2d$[122]	mp-3497 icds-52577	$CuFeS_2$	5.80	5.80	11.33	23.86	4.99	62.40	–3.572	–0.126
				5.87[a]	5.87[a]	11.20[a]	24.17[a]	–	–	–	–
				5.81[b]	5.81[b]	11.21[b]	–	–	–	–	
				5.80[c]	5.80[c]	11.35[c]	–	–	65[c],62[c]	–	–
Orthorhombic (OR)	$Pna2_1$[33]	mp-21459 icds-51618	β-$NaFeO_2$	6.69	6. 98	8,18	23.87	4.98	61.43	–3.570	–0.124
				6.69[a]	6.99[a]	8.27[a]	24.21[a]	–	–		
				6.68 [b]	6.99[b]	8.25[b]	–	–	–		
				6.81[d]	7.14[d]	8.33[d]	–	–	-	–	
Rhombohedral (RH)	$R\bar{3}m$[166]	mp-20162 icds-659385	α-$NaFeO_2$	3.76	3.76	18.75	19.15	6.21	82.94	–3.521	–0.075
				3.76[e]	3.76[e]	19.35[e]					
Monoclinic	$C2/m$[12]	mp-634855 icds-85317	$NaNiO_2$	6.55	3,76	6.59	20.02	5.94	65.78	–3.481	–0.035
Hexagonal	$P3m1$[156]	mp-7885 icds-25356	$LiMnSe_2$	4.48	4.48	5.30	23.02	5.17	63.96	–3.378	+0.068
Rocksalt	$Fm\bar{3}m$[225]	icds-165739	$CuAlS_2$	6.61	6.61	6.61	18.13	6.58	87.35	–3.058	+0.388

[a] Exp. [2]. [b] Exp. [4]. [c] Calc. [6]. [d] Calc. [5]. [e] Exp. [20]

calculated B_0 of 62 and 65 GPa [4]. We could not find any theoretical or experimental values for other phases for comparison.

At zero pressure and temperature we analyse the stability on the basis of the cohesive energy (E_{coh}) and formation energy (E_{for}). E_{coh} is defined as the energy required to separate the atoms infinitely far apart [40] while E_{for} is the energy difference between the cohesive energy of a solid and that of the its constituents in solid form [41,42]. Gherouel et al. [43] noted that in addition to OR-$AgInS_2$, the binary compounds Ag_2S and In_2S_3 could be present during the synthesis of CH-$AgInS_2$. We investigated the possible decomposition of $AgInS_2$ into the stable binary compounds Ag_2S [44] and In_2S_3 [45,46] according to the chemical reaction

$$AgInS_2 \rightarrow \frac{1}{2}Ag_2S + \frac{1}{2}In_2S_3.$$

The formation energy is:

$$E_{for}(InAgS_2^{sol})) = E_{coh}(AgInS_2^{sol}) - \frac{\left[\frac{1}{2}E_{coh}(Ag_2S^{sol}) + \frac{1}{2}E_{coh}(In_2S_3^{sol})\right]}{4}. \quad (1)$$

The lower the cohesive or the formation energy, the more stable the structure. As can be seen in Table 1, the cohesive energies are ordered as follows:

$$E_{coh}(I\bar{4}2d) < E_{coh}(Pna2_1) < E_{coh}(R\bar{3}m) < E_{coh}(C2/m) < E_{coh}(P3m1) < E_{coh}(Fm\bar{3}m),$$

suggesting that CH-$AgInS_2$ is the most stable structural phase of the compounds at zero pressure and temperature. It is also worth noting that CH-$AgInS_2$ and OR-$AgInS_2$ are energetically competitive phases with a well converged energy difference of about 20 meV. This is an indication that care should be taken while synthesising any of the two phases. The formation energies show the same trend as the cohesive energies. The rocksalt and the hexagonal phases have positive formation energies which indicate that, should it be possible to synthesise these phases, they will at best be meta-stable and are likely to dissociate into their binary solids.

An appropriate method for analysing the pressure phase transition at zero temperature is to make use of the enthalpy-pressure relation: $H = E_{coh} + PV$. A pressure phase transition occurs between two phases when, at a given pressure P_t, the enthalpy-pressure curves cross.

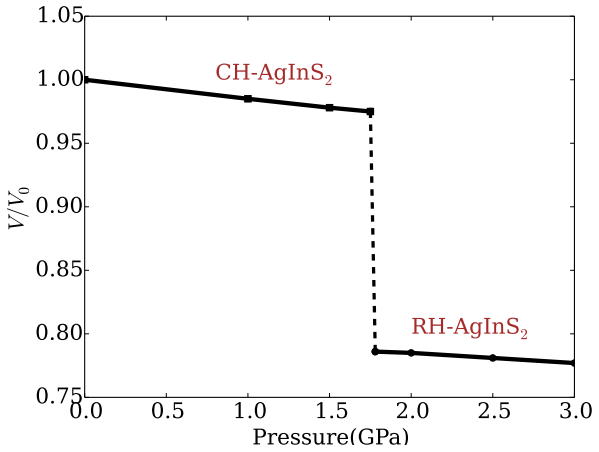

Fig. 2. Variation of the relative volume with pressure. V_0 is the equilibrium volume of the tetragonal phase at zero pressure and temperature.

The stable phase is the one with the lowest enthalpy. Figure 1b depicts the enthalpy versus pressure curves for all the structures under investigation. The competition between CH-$AgInS_2$ and OR-$AgInS_2$ can be noted once again, but CH-$AgInS_2$ remains the ground-state phase as previously predicted from the EOS. Within the numerical accuracy of our calculations, there is a possible phase transition from CH-$AgInS_2$ to the rhombohedral (RH-$AgInS_2$) phase around 1.78 GPa. Such a transition was observed experimentally by Range et al. [20], but at a pressure of 2 GPa. The volume of the two phases as a function of pressure is shown in Figure 2. A volume collapse of about 19.30% is observed at this transition pressure. The relaxed lattice parameters of RH-$AgInS_2$ at the transition pressure (1.78 GPa) are $a = 3.74$ Å, $c = 18.55$ Å which are within 5% relative error of the experimental values ($a = 3.76$ Å, $c = 19.35$ Å) obtained at 2 GPa [20].

As mentioned in the introduction, a number of studies suggested a high pressure rocksalt phase in chalcopyrite $CuAlX_2$ (X = S, Se, Te) materials [8,21,22]. We therefore extended our investigation up to 100 GPa to search for a high pressure rocksalt phase of $AgInS_2$. However, we found that the rhombohedral phase has the lowest enthalpy between 1.78 GPa and 93.5 GPa where a structural phase transition from a rhombohedral to a rocksalt phase takes place, as seen in Figure 1b. Such a high transition pressure is practically difficult to achieve, therefore we focus on the low pressure (0–2.5 GPa) phases, namely the chalcopyrite, the orthorhombic and the rhombohedral phases.

3.2 Dynamical and mechanical stabilities

We study the dynamical stability by investigating phonon dispersions at different pressures. Accurate force constants and phonon dispersion relations were computed using $2 \times 2 \times 2$ supercells based on the optimised structures at a given pressure using the VASP DFPT interface to the PHONOPY code [35,36]. A structure is dynamically stable when all the normal vibration modes have real and finite frequencies. Phonon dispersion curves along the high symmetry directions in the Brillouin zone are shown in Figure 3. The dispersion curves of CH-$AgInS_2$ and OR-$AgInS_2$ are above zero frequency as depicted in Figures 3a, 3d and 3f at 0, 1.78 and 2.5 GPa, respectively. Thus they are dynamically stable at these pressures. Figure 3g shows the phonon spectrum of RH-$AgInS_2$ at 0 GPa. Vibration modes with imaginary frequencies are seen near the Γ and the F points showing that RH-$AgInS_2$ at 0 GPa is dynamically unstable. Negligible imaginary modes are found at 1.78 GPa (seen in Fig. 3h) while only positive frequencies are observed at 2.5 GPa as depicted in Figure 3i.

Elastic constants were calculated to check for mechanical stability. Under stress, the total energy at volume V^*, in Voigt notation, is given by [47]:

$$E(\epsilon) = E(V^*, \epsilon = 0) + V^* \sum_i \sigma_i \epsilon_i + \frac{V^*}{2} \sum_{ij} C_{ij}(V^*) \varepsilon_i \epsilon_j + O(\epsilon^3), \quad (2)$$

where σ_i is the stress, ε_i is the strain and the C_{ij} are the elastic constants which correspond to the second derivative of the energy $E(\epsilon)$ with respect to the applied stress evaluated at V^*:

$$C_{ij} = \frac{1}{V^*} \left(\frac{\partial^2 E(\epsilon)}{\partial \epsilon_i \partial \epsilon_j} \right)_{V^*}. \quad (3)$$

When the applied stress is hydrostatic, the Born stability criteria [48–50] must be applied to the coefficients [51,52]

$$\tilde{C}_{\alpha\alpha} = C_{\alpha\alpha} - P; \quad \alpha = 1, 2, \ldots, 6; \quad \tilde{C}_{12} = C_{12} + P;$$
$$\tilde{C}_{13} = C_{13} + P; \quad \tilde{C}_{23} = C_{23} + P; \quad \tilde{C}_{14} = C_{14}. \quad (4)$$

Note that in absence of the pressure, $\tilde{C}_{ij}$ and C_{ij} are equal. The stability conditions for a tetragonal system are [53]:

$$\tilde{C}_{11} - \tilde{C}_{12} > 0, \tilde{C}_{11} + \tilde{C}_{33} - 2\tilde{C}_{13} > 0$$
$$\tilde{C}_{ii} > 0, 2\tilde{C}_{11} + \tilde{C}_{33} + 2\tilde{C}_{12} + 4\tilde{C}_{13} > 0. \quad (5)$$

According to Mouhat and Coudert [48] the necessary and sufficient mechanical stability conditions for an orthorhombic system are:

$$\tilde{C}_{11}\tilde{C}_{22}\tilde{C}_{33} + 2\tilde{C}_{12}\tilde{C}_{13}\tilde{C}_{23} - \tilde{C}_{11}\tilde{C}_{23}^2 - \tilde{C}_{22}\tilde{C}_{13}^2 - \tilde{C}_{33}\tilde{C}_{12}^2 > 0$$
$$\tilde{C}_{ii} > 0, \tilde{C}_{11}\tilde{C}_{22} - \tilde{C}_{12}^2 > 0, \quad (6)$$

while for a rhombohedral structure the following conditions have to be satisfied [48]

$$\tilde{C}_{11} - \tilde{C}_{12} > 0, \quad \left(\tilde{C}_{11} + \tilde{C}_{12}\right)\tilde{C}_{33} - 2\tilde{C}_{13}^2 > 0$$
$$\tilde{C}_{44} > 0, \quad \left(\tilde{C}_{11} - \tilde{C}_{12}\right)\tilde{C}_{44} - 2\tilde{C}_{14}^2 > 0. \quad (7)$$

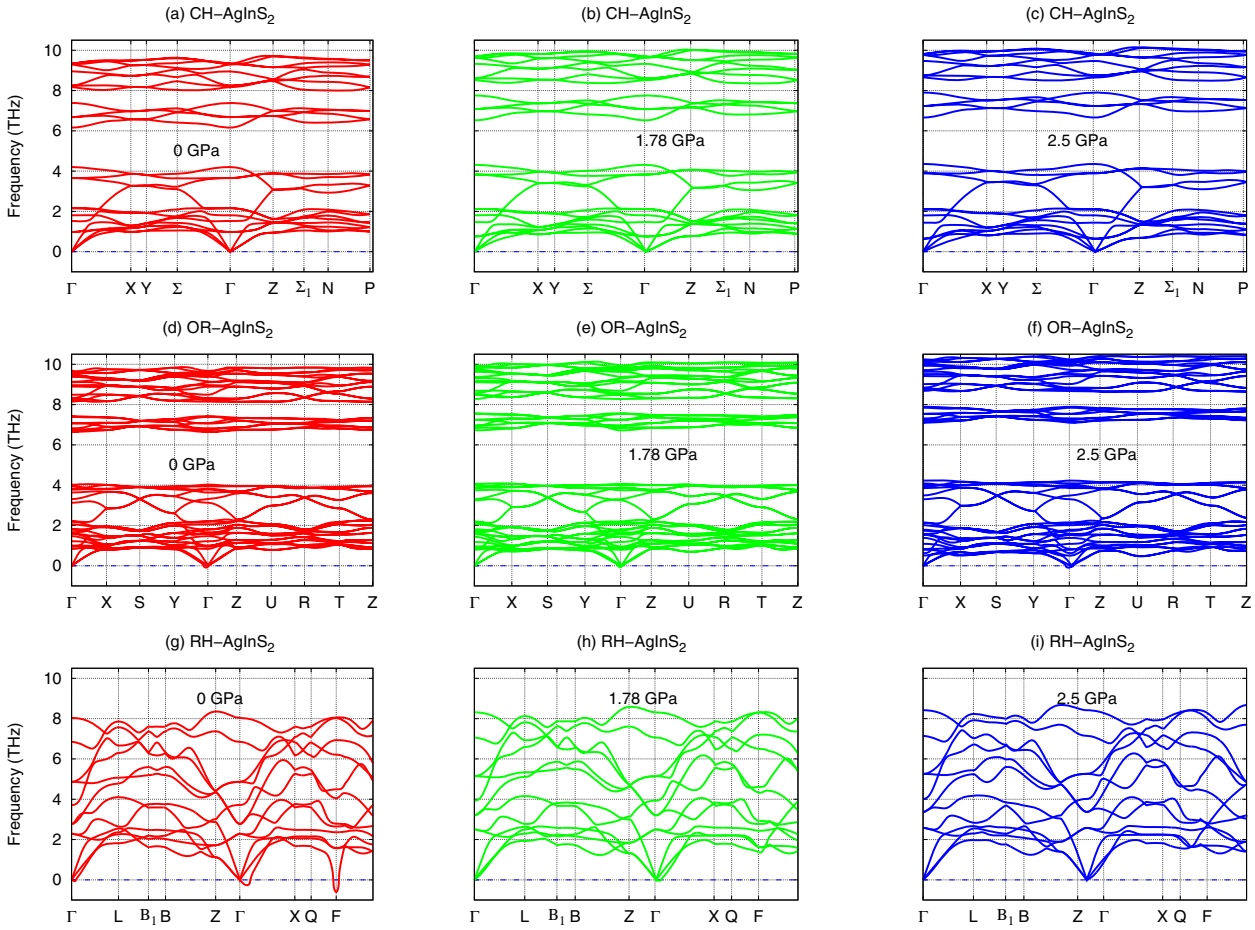

Fig. 3. $AgInS_2$ phonon dispersion curves at different pressures. Negative frequencies observed around the Γ and the F points of the rhombohedral structure at zero pressure are an indication of instability.

Bulk and shear moduli can be expressed respectively as follows:

$$B_V = \frac{1}{9}\left[(\tilde{C}_{11}+\tilde{C}_{22}+\tilde{C}_{33})+2(\tilde{C}_{12}+\tilde{C}_{13}+\tilde{C}_{23})\right],$$
$$G_V = \frac{1}{15}\left[(\tilde{C}_{11}+\tilde{C}_{22}+\tilde{C}_{33})-(\tilde{C}_{12}+\tilde{C}_{13}+\tilde{C}_{23})+3\tilde{C}'\right]$$
$$\text{with } \tilde{C}' = (\tilde{C}_{44}+\tilde{C}_{55}+\tilde{C}_{66}). \quad (8)$$

Elastic constants and moduli are presented in Table 2. In order to confirm the reliability of our elastic constants calculations, we compared our results with other calculated results for CH-$AgInS_2$ at 0 GPa, the only results available. We are not aware of any experimental data. Fairly good agreement is found between our calculated elastic constants for CH-$AgInS_2$ and those reported by Verma et al. [54]. The notable differences could be attributed to the different calculation methods and pseudopotentials used.

The chalcopyrite structure satisfy the mechanical stability criteria as stated above at all three pressures at which calculations were performed. For the case OR-$AgInS_2$, the stability criteria in equation (6) are satisfied. Their elastic constants C_{11}, C_{22}, C_{33}, C_{12}, C_{13} and C_{23} increase with increasing pressure while C_{44},C_{55} and C_{66} decrease. For the rhombohedral structure, the two first conditions in equation (7) are satisfied at all the pressures. At 0 GPa and 1.78 GPa, $C_{44} < 0$, hence $\tilde{C}_{44} < 0$ and $(\tilde{C}_{11}-\tilde{C}_{12})\tilde{C}_{44}-2\tilde{C}_{14}^2 < 0$. It follows that RH-$AgInS_2$ is mechanically unstable at 0 GPa and 1.78 GPa.

Bulk moduli are also calculated and listed in Table 2. However, because of the instability of RH-$AgInS_2$ at low pressure, the bulk moduli were only reported at 2.5 GPa. The bulk moduli are consistent with those obtained from the equation of state for all the structures (in brackets) or previously calculated values. It can be noted that the bulk moduli increase with pressure as expected. Poisson's ratio ν is associated with the nature of the atomic bonding. For all three structures, ν is greater than the critical value ($\nu \geq 0.25$) predicting an ionic character of the atomic bonding [55]. The G/B ratio is commonly used as a measure of brittleness and ductility of materials. According to the Pugh criteria [56,57], a typical brittle material should have $G/B \geq 0.5$, otherwise the material is ductile. Overall, the structures have $G/B < 0.5$ indicating that the materials are ductile. The Young moduli E are also reported in Table 2. At zero pressure, E (CH-$AgInS_2$) > E (OR-$AgInS_2$) suggesting that CH-$AgInS_2$ is stiffer than OR-$AgInS_2$. It is also worth noting that E decreases under

Table 2. Elastic constants C_{ij} (GPa), bulk moduli B (GPa), shear moduli G (GPa), Young's moduli E (GPa), Poisson's ratio ν and G/B for CH-$AgInS_2$, OR-$AgInS_2$ and RH-$AgInS_2$ at 0, 1.78 and 2.5 GPa.

Pres (GPa)	Phase	C_{11}	C_{22}	C_{33}	C_{12}	C_{13}	C_{23}	C_{14}	C_{44}	C_{55}	C_{66}	B	G	G/B	E	ν
	CH-$AgInS_2$	76		75	57	56			23		24	63	18	0.28	49	0.37
		79[c],84[f]		79[c],97[f]	64[c],52[f]	64[c],61[f]			18[c],23[f]		22[c],28[f]	69[c],62[c]	13[c]	0.19[c]	36[c]	0.41[c]
0	OR-$AgInS_2$	97	79	84	46	46	53		13	14	15	61	16	0.26	44	0.38
	RH-$AgInS_2$	123		111	61	70		15	−20		−13					
	CH-$AgInS_2$	82		80	67	64			20		23	70	16	0.22	45	0.39
1.78	OR-$AgInS_2$	102	80	85	55	56	61		12	12	14	68	14	0.20	39	0.40
	RH-$AgInS_2$	124		124	73	78		9	−1		2					
	CH-$AgInS_2$	84		82	69	67			18		22	73	15	0.20	42	0.40
2.5	OR-$AgInS_2$	106	81	89	63	63	69		11	9	12	74	12	0.16	34	0.42
	RH-$AgInS_2$	135		124	70	73		8	5		34	91	21	0.23	58	0.39

[c] Calc. [6]. [f] Calc. [54].

the effect of pressure and at 2.5 GPa, RH-$AgInS_2$ becomes the stiffest amongst the three structures.

3.3 Electronic and optical properties

We investigated the electronic properties by analysing the band structures and density of states (DOS). The GGA-PBEsol predicted a zero pressure bandgaps of 0.27 eV and 0.40 eV for CH- and OR-$AgInS_2$ respectively while RH-$AgInS_2$ has a metallic character. These values are very small when compared to the experimental values which are 1.86 eV and 1.98 eV, respectively [12]. This is a well known problem in the DFT community; employing a semilocal functional such as GGA-PBEsol can lead to the under-estimation of bandgaps. More reliable bandgaps were obtained by means of the meta-GGA MBJ functional, known to give a reasonable estimate of bandgaps for a wide range of materials [58,59]. It predicts bandgaps of 1.73 eV and 2.08 eV at 0 GPa for CH-$AgInS_2$ and OR-$AgInS_2$ respectively, which are in the range of their experimental values. RH-$AgInS_2$ changes from metal to semiconductor when the GGA-PBEsol exchange correlation potential is replaced by the MBJ approximation with a 2.5 GPa bandgap of about 0.95 eV. As we mentioned before, some structural measurements were done on RH-$AgInS_2$, but we are not aware of any previous experimental or theoretical work that determined its bandgap. As seen in Figure 4, we note that the bandgaps of CH-$AgInS_2$ and OR-$AgInS_2$ increase with increased pressure for both the GGA-PBEsol and MBJ potentials. Using GGA-PBEsol, RH-$AgInS_2$ is not sensitive to the effect of the pressure, remaining metallic at all pressures, but with MBJ a decrease of the bangap can be noted.

The bandstructures and the density of states (DOS) are depicted in Figures 5–7. The calculations were performed without inclusion of spin orbit coupling since it does not have a large impact on the electronic properties of sulfur based chalcopyrite materials [9,60]. The band structures are plotted along the high symmetry directions in the Brillouin zone and show that these compounds are direct bandgap materials. The bandgaps of CH-$AgInS_2$ and OR-$AgInS_2$ occur at the Γ point and for RH-$AgInS_2$

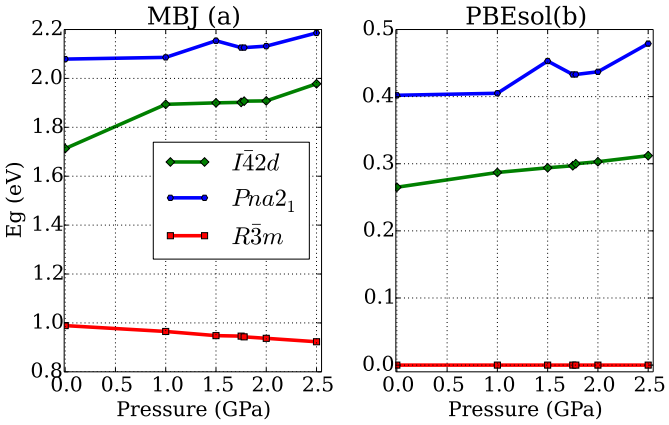

Fig. 4. Pressure dependant bandgap of the CH-, OR- and RH-$AgInS_2$.

it is at the F point. The spin polarized DOS's presented in Figures 5b, 6b and 7b show that the spin up and spin down DOS's are symmetric indicating that these compounds are non-magnetic. Partial DOS show similar features for OR-$AgInS_2$ and CH-$AgInS_2$, but that of RH-$AgInS_2$ looks different, despite the fact that all three compounds have the same atomic coordination. We observe that the shortest distance between Ag and In is 4.05 Å and 3.98 Å for CH-$AgInS_2$ and OR-$AgInS_2$ respectively, but for RH-$AgInS_2$ it is more than twice as large at (9.22 Å). This difference in the atomic environment of RH-$AgInS_2$ could explain the contrast in the partial DOS. For all the structures, the uppermost valence band is dominated by the Ag-d and S-p orbitals. The minimum of the conduction band has mainly S-s, S-p and In-s character. These features are usually observed in chalcopyrite materials [9,61,62].

The absorption coefficient α is a key property of a material since it measures the amount of light that can be absorbed by a given medium. It can be described by Beer's law [63]:

$$I(z) = I_0 e^{-\alpha z} \tag{9}$$

where I_0 the initial light intensity. Theoretically, it can be obtained from the frequency dependent dielectric function

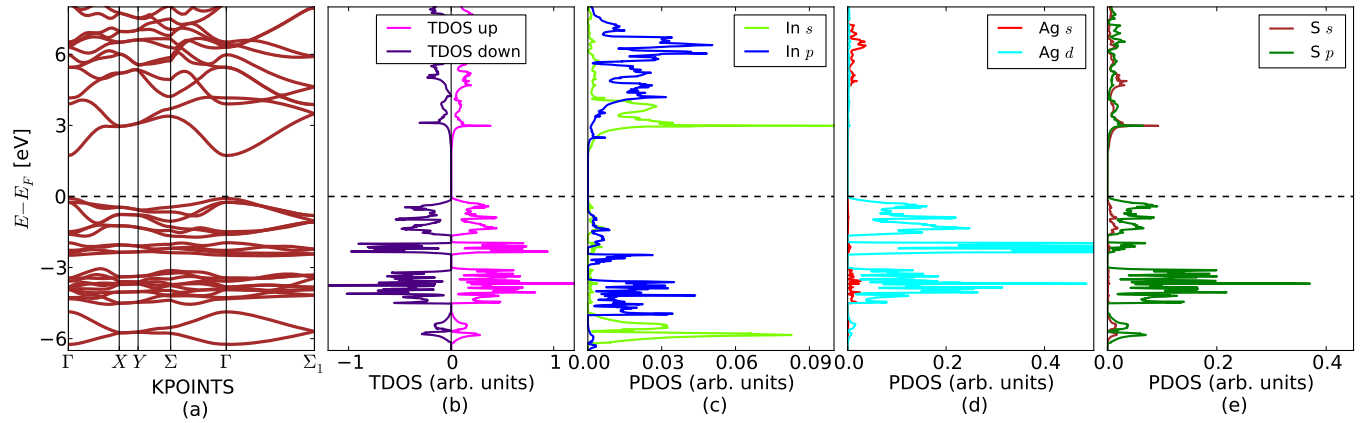

Fig. 5. Bandstructure, total and partial density of states of the CH-$AgInS_2$ structure at 0 GPa. Note that because of the small contribution to the bangap coming from the In atoms, the scale on the x-axis was changed.

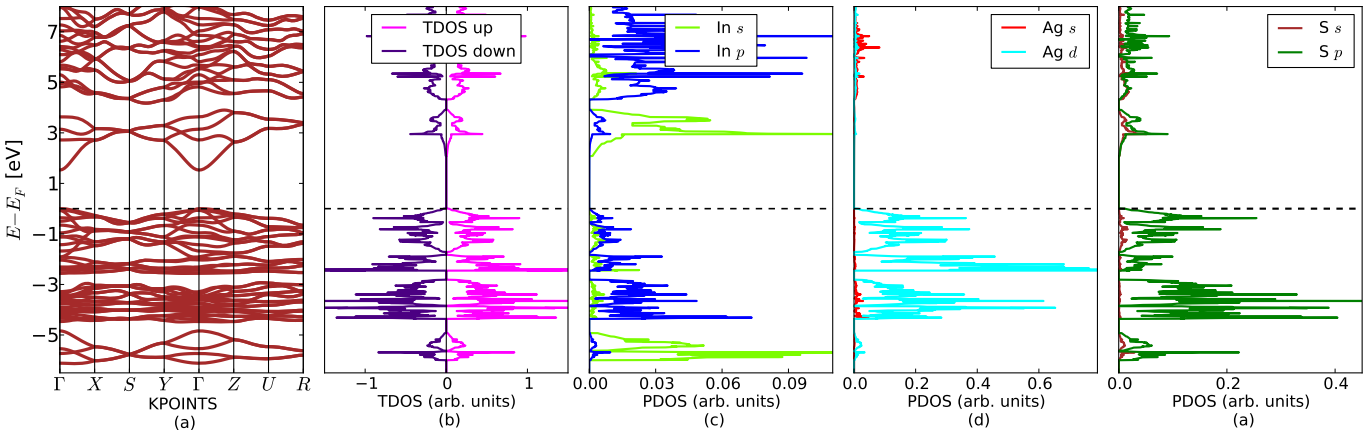

Fig. 6. Bandstructure, total and partial density of states of the OR-$AgInS_2$ structure at 0 GPa.

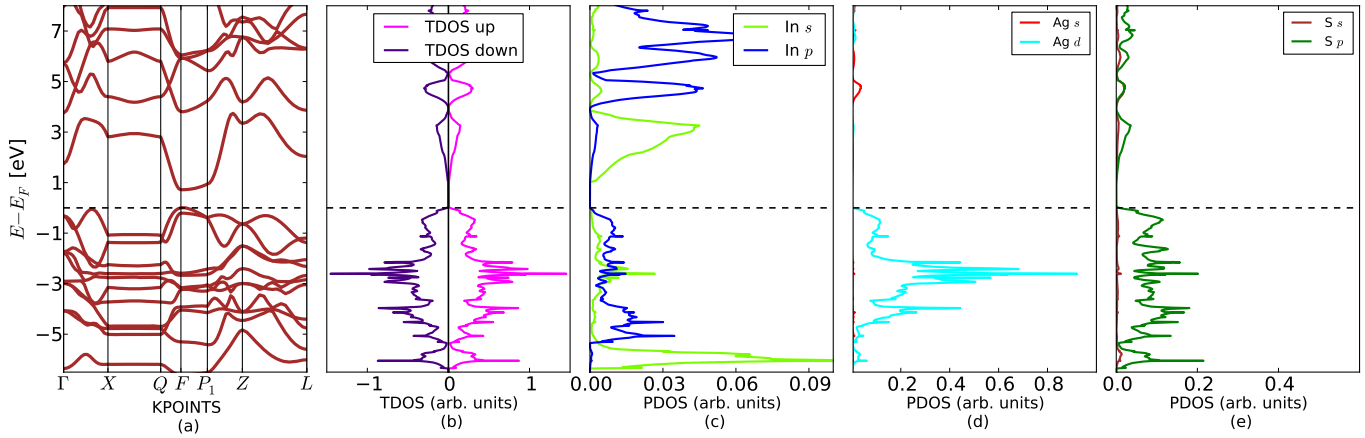

Fig. 7. Bandstructure, total and partial density of states of the RH-$AgInS_2$ structure at 2.5 GPa.

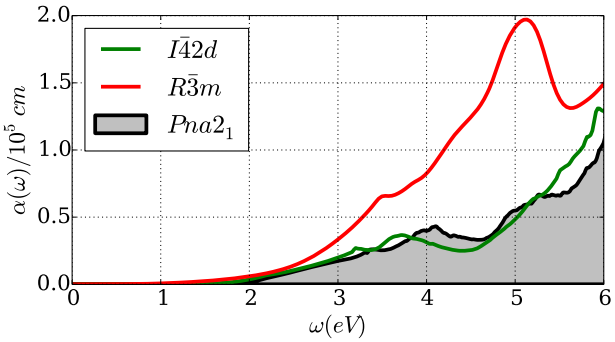

Fig. 8. Imaginary part of the dielectric of the three chalcopyrite structure ($I\bar{4}2d$) and the orthorhombic structure($Pna2_1$) at 0 GPa and rhombohedral structure($R\bar{3}m$) at 2.5 GPa.

using the relation

$$\alpha(\omega) = \sqrt{2}\omega\left[\left(\varepsilon_1^2(\omega) + \varepsilon_2^2(\omega)\right)^{\frac{1}{2}} - \varepsilon_1(\omega)\right]^{\frac{1}{2}} \qquad (10)$$

where ε_1 and ε_2 are respectively the real and the imaginary part of the dielectric function. Calculations for the absorption coefficient were performed within the random phase approximation with local fields included using MBJ. In Figure 8 the absorption spectra of the three compounds are shown for ω from 0 to 6 eV. The absorption threshold for CH-$AgInS_2$ and OR-$AgInS_2$ occurs at 1.27 and 2.07 eV, respectively. The maximum absorption for CH-$AgInS_2$ and OR-$AgInS_2$ are in the visible range at 0.26×10^5 cm^{-1} and 0.22×10^5 cm^{-1}, respectively. RH-$AgInS_2$ starts absorbing light in the infra-red region at 0.95 eV. At the edge of the visible range (3.1 eV), it reaches an absorption of 0.4×10^5 cm^{-1} and a very sharp peak located around 5.13 eV can be observed in the spectrum. The high absorption in the visible range could make RH-$AgInS_2$ more suitable for solar application compared to the other structures.

4 Conclusion

The aim of this work was to investigate the structural, mechanical, dynamical and electronic properties of the ternary chalcogenide materials $AgInS_2$ using ab initio techniques. The effect of the pressure on these properties was carried out at selected pressure of 0, 1.78 and 2.5 GPa. Six potential different phases of $AgInS_2$ were investigated. Using the cohesive energy, we found that the chalcopyrite phase was the most energetically favoured stable structure at zero pressure and temperature although the energy difference with the orthorhombic phase was very small. The variation of enthalpy with respect to pressure confirmed that the chalcopyrite was the zero pressure and temperature structure. It also showed that a pressure-induced phase transition from the chalcopyrite to the rhombohedral occurs around 1.78 GPa. This prediction is in agreement with the experimental report by Range et al. [20] at 2 GPa. A rocksalt phase occurs at 93.5 GPa contrary to the expectation around 15 GPa. The high pressure made this phase practically difficult to achieve. We also found a positive formation energy for the hexagonal and rocksalt phases which suggest that they are more likely to decompose into their elementary constituents. The chalcopyrite and the orthorhombic phases remained mechanically and dynamically stable at the selected pressure of our interest while the rhombohedral structure was only stable above the transition pressure. With the use of the new modified Becke-Johnson potential MBJ, we were able to predict accurately the bandgap of the chalcopyrite and the orthorhombic structures. For the first time, electronic properties of the rhombohedral structure were investigated and found that it has a bandgap of about 0.95 eV. Overall, the electronic properties were slightly sensible to the effect of the pressure.

This work was funded by the African Institute for Mathematical Sciences (AIMS) and the DAAD under Grant No. A/14/90078. The Centre for High Performance Computing (CHPC) is thanked for the computational resources.

References

1. J.E. Jaffe, A. Zunger, Phys. Rev. B **29**, 1882 (1984)
2. G. Delgado, A.J. Mora, C. Pineda, T. Tinoco, Mater. Res. Bull. **36**, 2507 (2001)
3. A.A. Vaipolin, Yu.V. Rud, I.V. Rozhdestvenskaya, Cryst. Res. Technol. **23**, 337 (1988)
4. J. Krustok, J. Raudoja, M. Krunks, H. Mandar, H. Collan, J. Appl. Phys. **88**, 205 (2000)
5. J. Liu, S. Chen, Q. Liu, Y. Zhu, Y. Lu, Comp. Mater. Sci. **91**, 159 (2014)
6. S. Sharma, A.S. Verma, V.K. Jindal, Physica B **438**, 97 (2014)
7. A.S. Verma, S.R. Bhardwaj, J. Phys.: Condens. Matter **19**, 026213 (2007)
8. V. Jayalakshmi, S. Davapriya, R. Murugan, B. Palanivel, J. Phys. Chem. Solids **67**, 669 (2006)
9. G.M. Dongho Nguimdo, D.P. Joubert, Eur. Phys. J. B **88**, 113 (2015)
10. J. Han, Z. Liu, K. Guo, J. Ya, Y. Zhao, X. Zhang, T. Hong, J. Liu, ACS Appl. Mater. Interfaces **6**, 17119 (2014)
11. Y. Wang, Q. Zhang, Y. Li, H. Wang, Nanoscale **7**, 6185 (2015)
12. D. Huang, C. Persson, Chem. Phys. Lett. **591**, 189 (2014)
13. C.H. Wang, K.W. Cheng, C.J. Tseng, Sol. Energy Mater. Sol. Cells **95**, 453 (2011)
14. K.W. Cheng, P.H. Liu, Sol. Energy Mater. Sol. Cells **95**, 1859 (2011)
15. C.J. Tseng, C.H. Wang, K.W. Cheng, Sol. Energy Mater. Sol. Cells **96**, 33 (2012)
16. Q. Cheng, X. Peng, C.K. Chan, ChemSusChem **6**, 102 (2013)
17. J.S. Jang, P.H. Borse, J.S. Lee, S.H. Choi, H.G. Kim, J. Chem. Phys. **128**, 154717 (2008)
18. C.A. Arredondo, J. Clavijo, G. Gordillo, J. Phys.: Conf. Ser. **167**, 012050 (2009)

19. H. Nakamura, W. Kato, M. Uehara, K. Nose, T. Omata, S. Otsuka-Yao-Matsuo, M. Miyazaki, H. Maeda, Chem. Mater. **18**, 3330 (2006)
20. K.J. Range, G. Engert, A. Weiss, Sol. Stat. Commun. **7**, 1749 (1969)
21. A. Werner, H.D. Hochheimer, A. Jayaraman, Phys. Rev. B **23**, 3836 (1981)
22. A. Abdellaoui, M. Ghaffour, M. Bouslama, S. Benalia, A. Ouerdane, B. Abidri, Y. Monteil, J. Alloys Compd. **487**, 206 (2009)
23. G. Kresse, J. Furthmüller, Comput. Mater. Sci. **6**, 15 (1996)
24. G. Kresse, D. Joubert, Phys. Rev. B **59**, 1758 (1999)
25. J.P. Perdew, A. Ruzsinszky, G.I. Csonka, O.A. Vydrov, G.E. Scuseria, L.A. Constantin, X. Zhou, K. Burke, Phys. Rev. Lett. **100**, 136406 (2008)
26. F. Tran, P. Blaha, Phys. Rev. Lett. **102**, 226401 (2009)
27. A.P. Gaiduk, V.N. Staroverov, J. Chem. Phys. **131**, 044107 (2009)
28. J. Heyd, G.E. Scuseria, M. Ernzerhof, J. Chem. Phys. **118**, 8207 (2003)
29. M. Shishkin, G. Kresse, Phys. Rev. B **75**, 235102 (2007)
30. A. Jain et al., APL Materials **1**, 011002 (2013)
31. A. Belsky, M. Hellenbrandt, V.L. Karen, P. Luksch, Acta Crystallogr. B **58**, 364 (2002)
32. F. Arab, F.A. Sahraoui, K. Haddadi, L. Louail, Comput. Mater. Sci. **65**, 520 (2012)
33. H.J. Monkhorst, J.D. Pack, Phys. Rev. B **13**, 5188 (1976)
34. S. Baroni, S. De Gironcoli, A. Dal Corso, P. Giannozzi, Rev. Mod. Phys. **73**, 515 (2001)
35. A. Togo, I. Tanaka, Scr. Mater. **108**, 1 (2015)
36. *Vasp-dfpt and phonopy calculation*, http://phonopy.sourceforge.net/vasp.html#vasp-dfpt-interface
37. W. Setyawan, S. Curtarolo, Comp. Mater. Sci. **49**, 299 (2010)
38. F. Birch, Phys. Rev. **71**, 809 (1947)
39. A. Zunger, J. Jaffe, Phys. Rev. Lett. **51**, 662 (1983)
40. M.S.H. Suleiman, Ph.D. thesis, University of the Witwatersrand Johannesburg, 2013
41. E.N. Orisakwe, V. Sharma, J.E. Lowther, Phys. Stat. Sol. B **249**, 1020 (2012)
42. S.K. Jain, P. Srivastava, Eur. Phys. J. B **86**, 389 (2013)
43. D. Gherouel, I. Gaied, M. Amlouk, J. Alloys Compd. **566**, 147 (2013)
44. A.J. Frueh, Zeitschrift für Kristallographie-Crystalline Materials **110**, 136 (1958)
45. N.S. Rampersadh, A.M. Venter, D.G. Billing, Physica B **350**, E383 (2004)
46. G. Steigmann, H. Sutherland, J. Goodyear, Acta Crystallogr. **19**, 967 (1965)
47. T. Hammerschmidt, I. Abrikosov, D. Alfe, S. Fries, L. Höglund, M. Jacobs, J. Koßmann, X.G. Lu, G. Paul, Phys. Stat. Sol. B **251**, 81 (2014)
48. F. Mouhat, F.X. Coudert, Phys. Rev. B **90**, 224104 (2014)
49. M. Born, Math. Proc. Cambridge Philos. Soc. **36**, 160 (1940)
50. D.C. Wallace, *Thermodynamics of Crystals* (Courier Corporation, 1998)
51. O. Gomis et al., J. Appl. Phys. **116**, 133521 (2014)
52. G. SinKo, N. Smirnov, J. Phys.: Condens. Matter **14**, 6989 (2002)
53. H. Zhai, X. Li, J. Du, Mater. Trans. **53**, 1247 (2012)
54. A.S. Verma, S. Sharma, R. Bhandari, B. Sarkar, V. Jindal, Mater. Chem. Phys. **132**, 416 (2012)
55. J. Haines, J. Leger, G. Bocquillon, Ann. Rev. Mater. Res. **31**, 1 (2001)
56. G.S. Manyali, R. Warmbier, A. Quandt, J.E. Lowther, Comput. Mater. Sci. **69**, 299 (2013)
57. S.F. Pugh, The London, Edinburgh Dublin Philos. Magazine J. Sci. **45**, 823 (1954)
58. D. Koller, F. Tran, P. Blaha, Phys. Rev. B **83**, 195134 (2011)
59. J. Camargo-Martinez, R. Baquero, Phys. Rev. B **86**, 195106 (2012)
60. S.H. You, K.J. Hong, B.J. Lee, T.S. Jeong, C.J. Youn, J.S. Park, S.N. Baek, J. Cryst. Growth **245**, 261 (2002)
61. I. Aguilera, J. Vidal, P. Wahnón, L. Reining, S. Botti, Phys. Rev. B **84**, 085145 (2011)
62. J.E. Jaffe, A. Zunger, Phys. Rev. B **29**, 1882 (1984)
63. M. Fox, in *Quantum Optics: An Introduction* (Oxford University Press, 2006), Vol. 6